Exploring Flood Predictability in Taiwan Through Coupled Atmospheric-Hydrological and High-Performance Hydrodynamic Models

Min-Hun Chi,[a] Chia-Jeng Chen,[b] Shih-Chieh Kao,[c] and Jian-Jun Liu[b]

[a] *AUO Corporation, 1 Machang Road, Taichung 42143, Taiwan*

[b] *National Chung Hsing University, 145 Xingda Road, Taichung 40227, Taiwan*

[c] *Oak Ridge National Laboratory, P.O. Box 2008, MS 6038, Oak Ridge, TN 37831-6038*

Corresponding author: Chia-Jeng Chen, cjchen@nchu.edu.tw

ABSTRACT

Effective flood simulation capabilities can tremendously support early warning and disaster prevention. To examine the applicability of a fully physics-based and high-performance flood simulation and forecasting modeling framework for a flood-prone region in Taiwan, we conduct a numerical experiment that couples the Weather Research and Forecasting model (WRF), WRF-Hydrological modeling system (WRF-Hydro), and the Two-dimensional Runoff Inundation Toolkit for Operational Needs (TRITON) to perform integrated rainfall, streamflow, and flood simulations. We first use the coupled WRF and WRF-Hydro (WWH) to predict rainfall and streamflow, and then drive TRITON with the predicted streamflow hydrographs to simulate flood depth and inundation area. With the refined spatial resolution and parameterization, this framework can better predict rainfall with reasonable spatial patterns. Although WWH could overestimate the amount of rainfall in some areas, the uncertain rainfall-streamflow predictions produce reasonable flood maps able to pinpoint regions at risk of flooding. In terms of model efficiency, the graphic processing unit-based computation can yield a speed-up factor as high as ~13 compared to the central processing unit-based computation, promoting the efficacy of the coupled modeling framework in practical real-time flood forecasting.

SIGNIFICANCE STATEMENT

The purpose of this study is to develop and assess a modeling framework that integrates a coupled atmospheric-hydrological model with a high-performance hydrodynamic model for rainfall, streamflow, and flood simulations in a holistic manner. By integrating these state-of-the-art models, we aim to advance our understanding of regional flood predictability subject to the chaotic nature of hydrometeorological forecasts. Based on our case study in Taiwan, we demonstrate that the proposed modeling framework can identify inundation hotspots despite the found uncertainties in rainfall-streamflow predictions. We also demonstrate that using the high-performance hydrodynamic model can significantly enhance simulation efficiency, suggesting the need for a modeling framework like the one proposed in this study for real-time flood forecasting.

1. Introduction

Abundant evidence indicates that the intensified precipitation and more frequent extreme events due to climate change have elevated the risk of flooding (Tabari, 2020; Huang et al., 2021; Wasko et al., 2021). Additionally, land use and land cover (LULC) changes, such as deforestation, can influence rainfall-runoff characteristics, thereby altering the severity and susceptibility of regional flooding (Chen et al., 2020; Janizadeh et al., 2021; Pal et al., 2022). With disastrous floods causing significant economic losses (Dottori et al., 2018), effective flood modeling and forecasting capabilities are crucial for establishing strategies for disaster prevention and relief (Cvetkovic and Martinović, 2020).

Contemporary flood prediction and hazard assessments rely heavily on various flood models rooted in mathematical equations and numerical techniques in hydraulics and hydrodynamics (Teng et al., 2017). Some of the most commonly used models include the Hydrologic Engineering Center's River Analysis System (HEC-RAS; Brunner, 2016), SOBEK, and FLO-2D (Yang et al., 2022). Advances in high-performance computing (HPC) and graphic processing units (GPUs) have stimulated a new wave of hydrodynamic model development, such as the Two-dimensional Runoff Inundation Toolkit for Operational Needs (TRITON; Morales-Hernández et al., 2020). As an open-source, shallow-water equations-based model, TRITON has been employed in various computationally demanding studies. For instance, Morales-Hernández et al. (2021) used TRITON to simulate the flood caused by Hurricane Harvey in the Gulf Coast region of the United States in 2017. They also demonstrated the computational efficiency of TRITON by evaluating the differences in simulation time under different hardware implementations (e.g., with or without GPU). Dullo et al. (2021) coupled the Distributed Hydrology Soil Vegetation Model (DHSVM) with TRITON to simulate streamflow and regional inundation in river basins in the Southeastern U.S. Li et al. (2021b) later applied the same coupled modeling framework as Dullo et al. (2021) to evaluate regional inundation in the South-Central region of the U.S.

One of the necessary inputs for flood models is the regional hydrometeorological conditions (e.g., rainfall, runoff, and streamflow). Using numerical weather prediction (NWP) and hydrological models to obtain such inputs has become a trending topic in flood simulation and forecasting (Eltahir and Bras, 1996; Asghar et al., 2019). Among various NWP systems designed for regional climate modeling, the Weather Research and Forecasting model (WRF, Skamarock et al., 2008) represents the state of the art and has been configured and adopted as an operational forecasting system by various agencies (e.g., the High-Resolution Rapid Refresh, HRRR; Dowell et al., 2022; James et al., 2022). Regarding advanced hydrological modeling, the WRF-Hydrological modeling system (WRF-Hydro), as an enhanced version of WRF's built-in hydrological model, can be directly coupled (fully, two-way) with WRF to explicitly account for land-atmosphere interactions. Numerous studies thus used WRF and WRF-Hydro for flood simulation and forecasting. For example, Lin et al. (2018) used WRF-Hydro to simulate the flood discharge variability during Hurricane Ike. They explored the efficiency of the computational framework to provide relevant information for future large-scale flood simulations. Papaioannou et al. (2019) used WRF and WRF-Hydro to simulate the hydrometeorological conditions of a flood event, which were further supplied to HEC-RAS to simulate the inundation of the Argolic River in Greece. Wehbe et al. (2019) used the coupled WRF-WRF-Hydro (WWH) model to evaluate the extreme weather event that affected the United Arab Emirates in March 2016. Galanaki et al. (2021) used the coupled WWH model to study the effects of land-atmosphere interactions on rainfall and flood forecasting in Attica, Greece. Varlas et al. (2021) used the coupled WWH model for rainfall forecasting in Greece from September 2015 to August 2019, followed by inundation simulation using HRC-RAS. The above studies have revealed that WRF-Hydro represents a versatile model that can be coupled with WRF to provide a more physical means for various simulation needs in the context of flood forecasting and water budget analysis (Chen et al., 2023).

According to the above literature review, high-performance hydrodynamic models (e.g., TRITON) and coupled atmospheric-hydrological models (e.g., WWH) have greatly benefited flood modeling and assessments. The former can vastly reduce the computing time for high-resolution inundation modeling, while the latter can provide a well-grounded estimate of regional hydrometeorological conditions. Therefore, using these models in an integrated fashion seems a straightforward and promising approach towards real-time flood forecasting. However, there is a shortage of studies exploring the use of these models, primarily due to a lack of experience and confidence in computational infrastructure development and model performance, respectively. To fill the knowledge gap, it is essential to integrate these modern models into a plausible framework where their capability and uncertainty can be assessed over a region with quality data (e.g., Taiwan). The implementation and feasibility of such a framework are imperative, especially under climate change scenarios with a higher likelihood of the failure of flood protection measures (Kundzewicz et al., 2014).

In Taiwan, some flood-related studies have already been conducted using NWP and hydrological/hydraulic models. For instance, Hsiao et al. (2013) used WRF along with the

WASH123D model (WAterSHed Systems of the 1-D Stream-River Network, the 2-D Overland Regime, and the 3-D Subsurface Media) to conduct typhoon rainfall and flood ensemble prediction in the mountainous watersheds of Taiwan. Shih et al. (2014) later used WRF and WASH123D for rainfall-runoff prediction in Lanyang Plain (northeastern Taiwan) and attempted to dissect the variations of flood hydrographs. Yang et al. (2015) established the "Taiwan Cooperative Precipitation Ensemble Forecast Experiment," which aims to enhance flood forecasting and assess flood risk in Taiwan's urban areas. While these studies have established a strong foundation for refined flood simulation, the value of coupled atmospheric-hydrological models and high-performance hydrodynamic simulations has yet to be revealed. Further, one of the important aspects we aim to present in this study is to examine to what extent a regional flood could be predicted by imperfect precipitation and streamflow simulations. Extracting useful information from such imperfection for flood forecasting would be scientifically as significant as improving the accuracy/reliability of precipitation or streamflow forecasts, especially under no circumstances would quantitative precipitation forecasts (QPFs) be error-free.

To pave the way towards using coupled atmospheric-hydrological and high-performance hydrodynamic models for real-time flood forecasting, this study sets the following objectives: 1. As a proof of concept, we develop a modeling framework that couples WWH with TRITON for the simulation of rainfall, streamflow, and inundation in a flood-prone region of Taiwan. 2. We run and assess the simulations over selected heavy-to-torrential rainfall cases representing flood events of various rainfall types. 3. We evaluate the efficiency of TRITON in different hardware implementations. The proposed modeling framework is expected to not only unveil some complex mechanisms and interactions between hydrometeorology and flooding but also provide more rapid flood modeling capabilities for operational needs.

2. Materials

a. Study area

The study area is the Gaoping region, located in southwestern Taiwan and bounded by the Chianan Plain, Pingtung Plain, Central Mountain Range, and Taiwan Strait to the north, south, east, and west, respectively (Fig. 1). The main river in the region is the Gaoping River, which is the most extensive river system in Taiwan by drainage area (~3,257 km^2) and has several tributaries, including the Laonong, Qishan, Ailiao, and Meinong Rivers. The

Gaoping River basin shows a steep slope from northeast to southwest, from the high mountains above 3,500 meters to the low-lying plains. In contrast, there are some additional coastal river basins (e.g., the Erren River) in the western part of the Gaoping region, where the average slope is much milder. The Gaoping region has a tropical monsoon climate, with a rainy season spanning from June to August due to the prevalence of the southwestern summer monsoon and tropical cyclone. The spatial distribution of rainfall in the region is highly uneven, primarily due to the topographical effect and distinct weather systems. These hydro-climatological features make the Gaoping region one of the most flood-prone areas in Taiwan, as evidenced by many historical records of severe flooding. The high risk of flooding in the Gaoping region justifies its selection as the study area for this analysis.

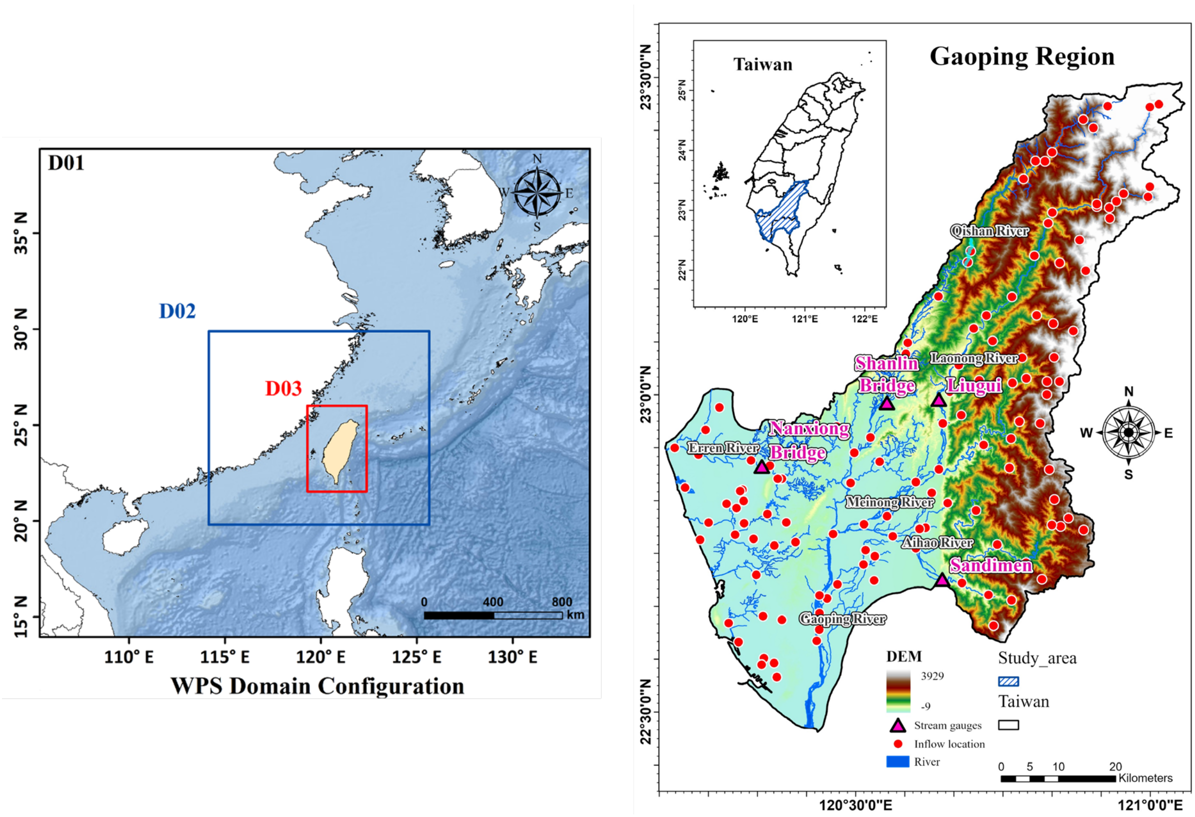

Fig. 1. WRF's three-level nested modeling domains (left) and the Gaoping region with the major tributaries and 126 inflow points specified in the Gaoping region, used to obtain simulated inflow hydrographs from WRF-Hydro as input data to TRITON for inundation simulation (right).

b. Elevation and land use data

In the pre-processing and simulation of WRF-Hydro, the HydroSHEDS product (Hydrological data and maps based on SHuttle Elevation Derivatives at multiple Scales;

Lehner et al., 2008) is adopted. The HydroSHEDS product was derived from the SRTM (Shuttle Radar Topography Mission) digital elevation model (DEM) at a resolution of 3 arc-seconds (~90 meters at the equator). The resolution and elevation accuracy of HydroSHEDS (~1 m) are sufficient for hydrological simulation to generate streamflow hydrographs. However, a finer and more accurate DEM is usually required for a two-dimensional (2D) inundation model such as TRITON. Thus, another 50-m DEM product is derived from the official product released by Taiwan's Ministry of the Interior. The 50-m DEM product has undergone hydrological conditioning/corrections using river cross-section data acquired from Taiwan's Water Resources Agency (WRA) and additional data to correct the original DEM (e.g., deepening and widening elevations along river channels and removing bridges and other facilities that may cause artificial backwater effect).

LULC data, another input required for WWH and TRITON simulations, is derived from the official product released by Taiwan's National Land and Survey Center (NLSC) in 2015. This realistic product was developed using cadastral and field surveys, aerial images, and GIS analysis. A series of GIS processing and land use ID conversions have been conducted to make the NLSC data compatible with the WRF environment (Chen et al., 2020; 2023). The LULC data is also used as a priori information to determine Manning's roughness coefficients in WRF-Hydro and TRITON.

c. Rainfall and streamflow data and case selection

Two gridded rainfall products are acquired from the Taiwan Climate Change Projection Information and Adaptation Knowledge Platform (TCCIP) to evaluate the performance of rainfall simulation, which is critical to the subsequent flood simulation. The first product is the gauge-based, best-available gridded rainfall data for Taiwan (Li et al., 2021a; Huang et al., 2022; Lee et al., 2023); in the development of this gridded dataset (1 km daily), TCCIP incorporated an immense amount of gauge data from many sources in Taiwan (e.g., Central Weather Agency, Water Resources Agency, and Environmental Protection Administration). We also use the gauge-based data to calibrate WRF-Hydro, which will be explained more in the next section. The second product is the model-based rainfall data, referred to as the Taiwan ReAnalysis Downscaling data (TReAD), developed by TCCIP's effort to dynamically downscale the ERA5 reanalysis dataset (ECMWF, 2017). TCCIP used WRF and Taiwan's local LULC data (Chen et al., 2019) for downscaling, and the resolution of TReAD (2 km, hourly) is adequate for a detailed comparison with our simulated rainfall.

Observed streamflow data acquired from WRA gauges are used for both the calibration of WRF-Hydro and flood forecasting. Table 1 lists the metadata information (e.g., coordinates and corresponding watershed) about the WRA gauges. Four representative cases of torrential rainfall are selected for our numerical experiment. The selection is based on the reports of disaster records and damage statistics compiled by Taiwan's National Science and Technology Center for Disaster Reduction (NCDR) for the Gaoping region. These cases include two typhoon events, one southwesterly flow event, and one plum rain event. The event type and period of each selected case are presented in Table 2.

ID	Gauge Name	Coordinates		Corresponding Watershed
		Latitude	Longitude	
1	Liugui	22.9958	120.6395	Gaoping River
2	Shanlin Bridge	22.9904	120.5510	Gaoping River
3	Nanxiong Bridge	22.8894	120.3382	Erren River
4	Sandimen	22.7125	120.6460	Gaoping River

Table 1. Metadata information regarding the Water Resources Agency streamflow gauges used in this study.

Case ID	Year	Rainfall Event	Event Period (Local Standard Time)
1	2009	Typhoon Morakot	08/07 00:00~08/08 24:00
2	2010	Typhoon Fanapi	09/19 00:00~09/20 24:00
3	2012	Southwesterly flow	06/10 00:00~06/11 24:00
4	2020	Plum rain	05/22 00:00~05/23 24:00

Table 2. Selected cases and corresponding event types and periods.

3. Methodology

a. WRF and configuration

This study utilizes WRF version 4.2.1 to carry out the simulations. As in several of our previous studies in Taiwan (e.g., Chen et al., 2020; Li et al., 2021a; Chen et al., 2023), WRF is run with three nested domains (Fig. 1) at different horizontal resolutions (i.e., 18, 6, and 2 km in D1, D2, and D3, respectively) and a stretched vertical grid consisting of 45 sigma levels. The parameterization schemes used in WRF are all set to be the same as those used in our previous studies (e.g., Betts-Millers-Janjic, YSU, RRTMG, and WSM5 for the cumulus, boundary layer, radiation, and microphysics parameterizations, respectively). The Noah land surface model (Livneh et al., 2011) is specified in our simulations. The National Centers for Environmental Prediction (NCEP) FNL (Final) Operational Global Analysis data is used to supply initial and boundary conditions. After completing each simulation, we take outputs from D3 for successive analysis.

b. WRF-Hydro and configuration

WRF-Hydro, as a community-based distributed hydrological model, can provide more accurate information on the redistribution between surface runoff, subsurface flow, and channel flow. WRF-Hydro has been developed to run in a standalone mode or to be coupled with WRF and other Earth system models (Gochis et al., 2020). The major physics behind WRF-Hydro entails several modeling components. For instance, the calculation of overland flow is based on the diffusive wave equation, simplified from the more general St. Venant equations of continuity and momentum. In terms of channel flow routing, the classic Muskingum-Cunge approach is used.

This study employs WRF-Hydro version 5.1.1. In the pre-processing of WRF-Hydro, the spatial resolution of routing grids and the minimum contributing area are determined as 100 m and 2 km^2 by setting the regridding factor as 20 and the number of routing grids to define a stream as 200, respectively. In addition, forecasting points are placed at the locations of the WRA gauges to facilitate the acquisition of streamflow simulation values. Before fully coupled WWH simulations, WRF-Hydro is run in a standalone mode to assess whether reasonable surface runoff can be generated subject to observed rainfall. The assessment involves calibrating WRF-Hydro's parameters, and associated results will be presented in Sec. 4.a.1.

c. TRITON and configuration

As discussed in Sec. 1, TRITON is an emerging open-source 2D hydrodynamic model known for its computational efficiency through multi-GPU acceleration. TRITON uses a conservative form of the 2D shallow water equations as the governing equations to calculate surface water movement. The equations, along with source terms, are solved using the finite volume method. The primary input data of TRITON include a DEM, surface roughness (i.e., Manning's n values, derived from a look-up table of different land use types), coordinates of inflow points, and time series of corresponding inflows. TRITON can also take localized runoff (i.e., effective rainfall derived from rain gauge observations or an NWP model) as the input data, which is essential for the simulation of pluvial flooding. TRITON offers a wide range of boundary conditions, from which an adequate one can be selected or to enable more convenient coupling with other models (e.g., coastal storm surge models). In this study, the normal slope boundary condition is specified over the coastline of the Gaoping region. More detailed technical descriptions of TRITON can be found in Morales-Hernández et al. (2021).

Overall, WRF-Hydro and TRITON represent the hydrological and hydraulic modeling components, respectively. Since the feedback from short-term surface inundation on weather and hydrologic systems is expected to be minor, a "one-way" coupled modeling strategy (e.g., Xia et al., 2019; Dullo et al., 2021) that passes streamflow hydrographs from hydrological models into hydraulics models can be adopted. In the Gaoping region, 126 inflow points are specified in Fig. 1; these points are mainly located at stream order 2 or 3, determined in the pre-processing of WRF-Hydro. The configuration of the simulation period follows our previous WRF and WWH applications in Taiwan (e.g., Chen et al., 2020; Chen et al., 2023). Each simulation begins at 0600 UTC (Day 0, 1400 local standard time, LST) one day ahead of the event and ends at 1800 UTC two days after (Day 3, 0200 LST), totaling 60 hours. The first ten simulation hours are taken as the model spin-up period, and outputs from the subsequent 48-hour period are used for analysis. It has been shown by previous studies (e.g., Chien et al., 2002; Hong, 2003; and Wang et al., 2017) that a short spin-up period is sufficient to develop realistic cloud and rainfall patterns from the large-scale initial condition with a satisfactory skill, especially for such a short-range simulation of torrential rainfall as ours (Chen et al., 2020; 2023). Fig. 2 presents the diagram of the proposed modeling framework.

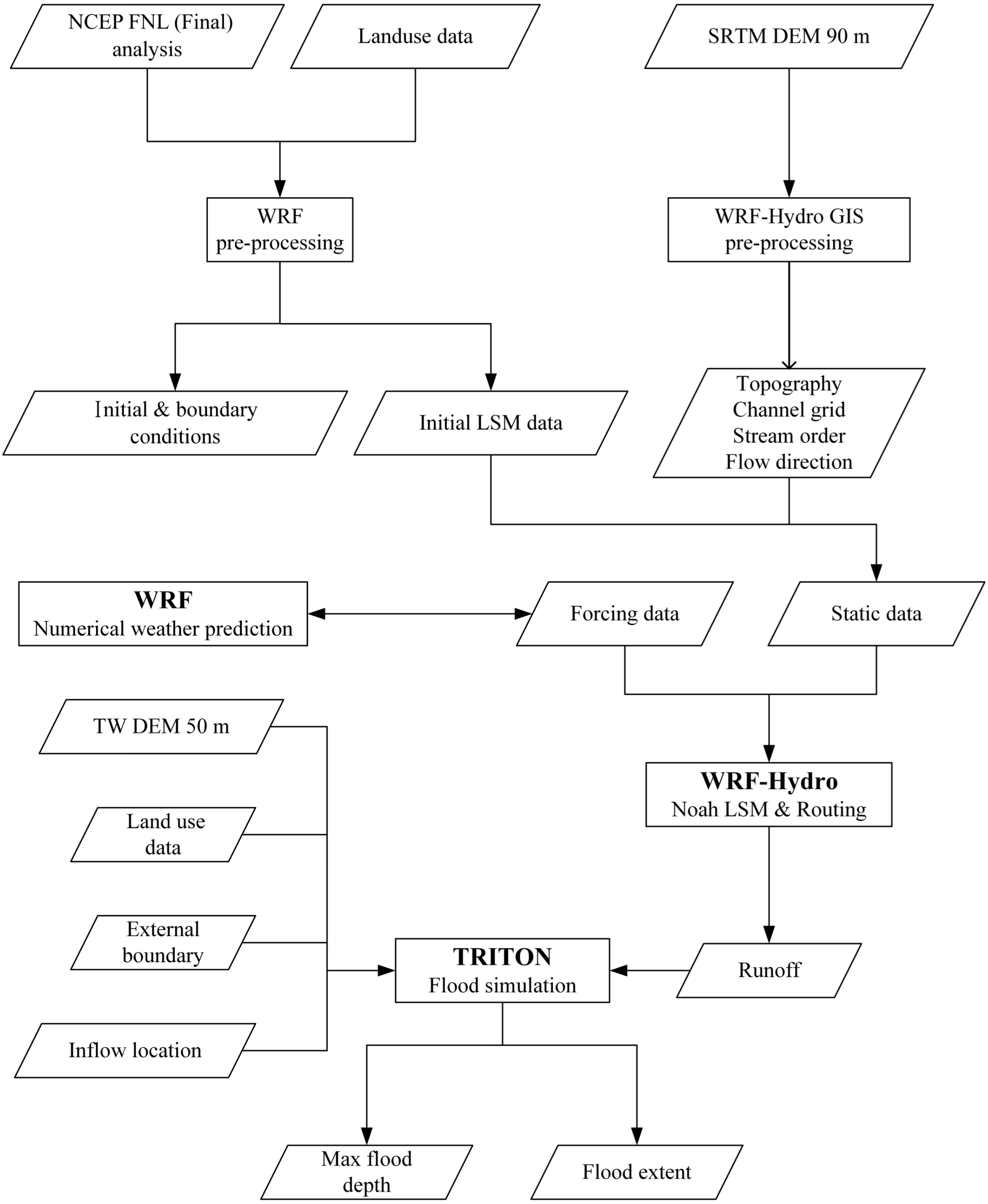

Fig. 2. Diagram of the proposed modeling framework.

4. Results and discussion

This section is divided into two parts to present the results. The first part covers the calibration of WRF-Hydro, followed by the evaluation of simulated rainfall and streamflow using the coupled WWH atmospheric-hydrological model. The second part assesses the simulation of inundation using WWH and TRITON in a one-way coupled modeling framework, and then illustrates TRITON's model efficiency under different grid resolutions and hardware implementations.

a. Coupled atmospheric-hydrological simulation

1) WRF-HYDRO CALIBRATION

To evaluate the reliability of WRF-Hydro in terms of streamflow simulation, it is first calibrated in standalone mode using observed meteorological forcing data. A wide range of parameters can be calibrated in WRF-Hydro, such as soil parameters, Manning's roughness coefficients, and soil hydraulic properties. According to Wang et al. (2020), modifying Manning's coefficients for different stream orders can significantly influence simulated streamflow, making it a priority for our calibration efforts. The calibration is performed using a stepwise approach similar to that proposed by Yucel et al. (2015). More detailed descriptions regarding the manual calibration can be found in our previous work (Chen et al., 2023). We have included a table listing sensitive parameters in WRF-Hydro that could be calibrated, along with their respective ranges (Table S1 in the supplemental material). It is important to note that, due to limited computational resources, our scope here is to achieve reasonable calibration. More comprehensive and automated calibration (e.g., Silver et al., 2017) should certainly be considered to further enhance WRF-Hydro's performance for operational forecasting.

In this study, the TCCIP precipitation data are used as the primary meteorological forcing, while other necessary meteorological forcings (e.g., temperature, air humidity, short-wave and long-wave radiation, and wind speed) and antecedent soil moisture states are obtained from a preliminary WWH run. Typhoon Morakot (Case 1 in Table 2), which caused unprecedented heavy rainfall in the Gaoping region, is adopted as the case for calibration. The calibrated streamflow hydrographs were compared with observed data, as shown in Fig. 3. The Nash-Sutcliffe Efficiency (NSE) between the calibrated and observed hydrographs at the Sandimen and Nanxiong Bridge stations are 0.88 and 0.63, respectively, indicating the "excellent" and "good" performance according to Moriasi et al. (2015). These credible hydrologic responses to heavy rainfall confirm the applicability of the calibrated WRF-Hydro model for the subsequent coupled atmospheric-hydrological simulation.

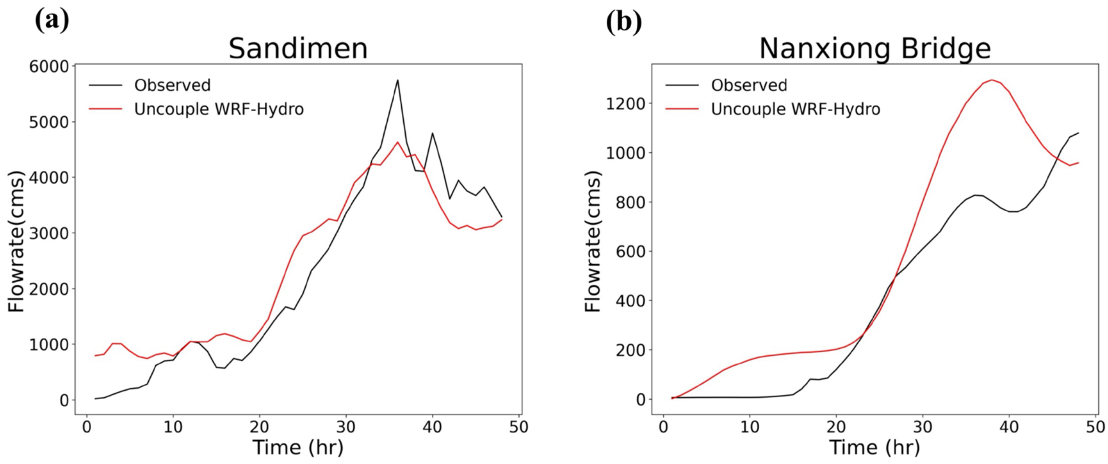

Fig. 3. Calibration results of WRF-Hydro, showing observed vs. simulated hydrographs using WRF-Hydro in a standalone mode for Typhoon Morakot (Case 1).

2) RAINFALL AND STREAMFLOW SIMULATIONS USING WWH

Figs. 4 to 7 show the spatial distributions of four rainfall events across Taiwan, using TCCIP precipitation data as the benchmark for evaluating the performance of the WWH simulation. The WRF-only and TReAD simulations are also included for comparison. To assess the performance of simulated rainfall amounts, the maximum cumulative rainfall per day for each rainfall event is listed in Table 3. In Case 1 (Typhoon Morakot), the WRF-only and WWH simulations produced spatial patterns comparable to the TCCIP data at the island scale, but they overestimated the amount of rainfall on the first day and underestimated on the second day. While the TReAD simulation produced more accurate rainfall patterns, an overall overestimation of rainfall is evident (Table 3). In Case 2, Typhoon Fanapi brought heavy rainfall, peaking at the eastern and southwestern parts of the island. All simulated rainfall patterns could mimic the rainfall peaks, yet the WRF-only and WWH simulations still overestimated the amount of rainfall in the eastern areas.

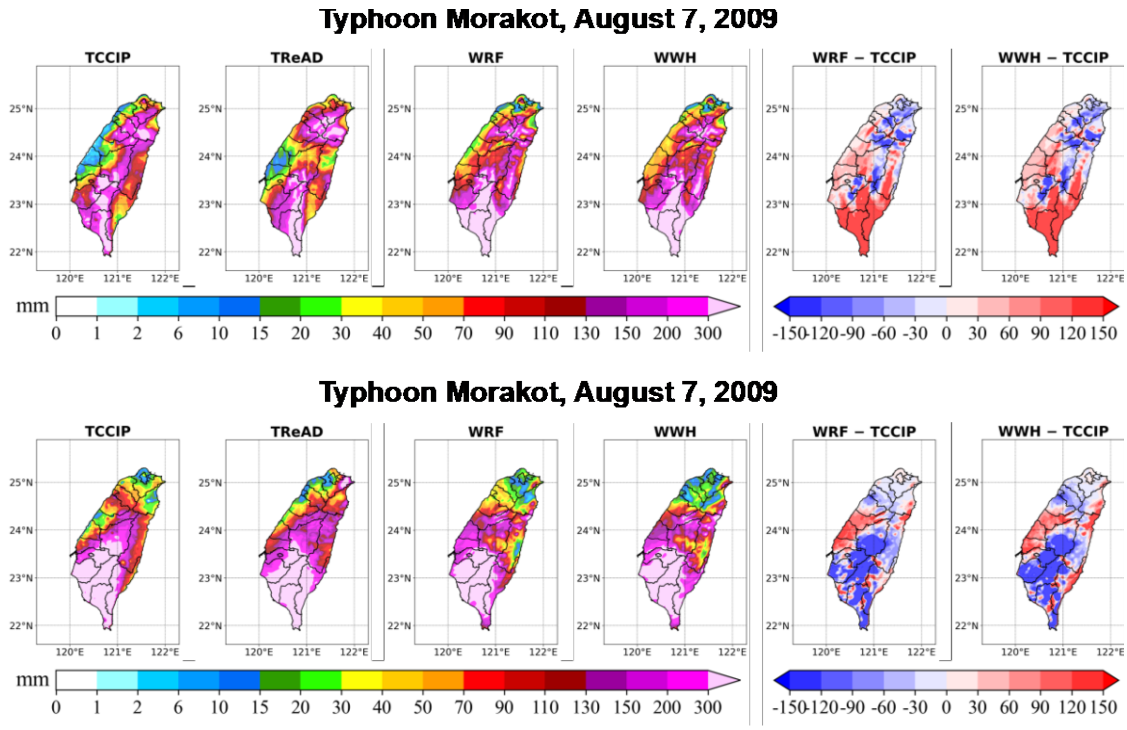

Fig. 4. Spatial distributions of TCCIP, TReAD, WRF-only (denoted as WRF), and coupled WRF-WRF-Hydro (WWH) cumulative rainfall on the two days of Typhoon Morakot (Case 1). Difference plots between the model simulation (WRF or WWH) and the reference products (TCCIP) are also shown.

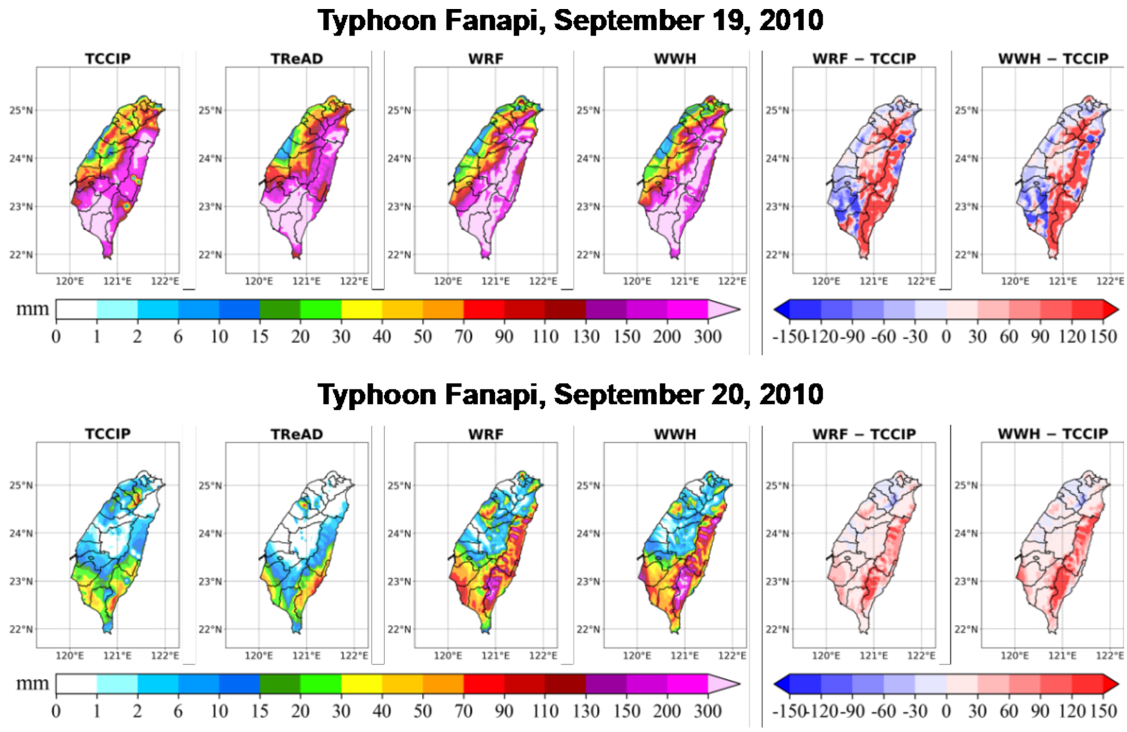

Fig. 5. As in Fig. 4, but for Typhoon Fanapi (Case 2).

In Case 3 (southwesterly flow), while the WRF-only and WWH simulations overestimated rainfall, the overestimation was relatively less pronounced than in Cases 1 and 2 on Day 1 (see Table 3). In contrast, the TReAD simulation appeared to miss the rainfall peak in the central region. In Case 4 (plum rain), local convection in the WRF-only and WWH simulations dissipated faster than the observed data, leading to underestimated rainfall in the southern mountainous areas on Day 2. On the other hand, the TReAD simulation performed better in terms of rainfall patterns and amounts during this event. In general, although the WRF-only and WWH simulations tend to overestimate rainfall in some cases, they can produce reasonable rainfall patterns comparable to those of TReAD and TCCIP at the island scale. When focusing on the Gaoping region, biases in rainfall amounts and deviations in spatial patterns become more evident.

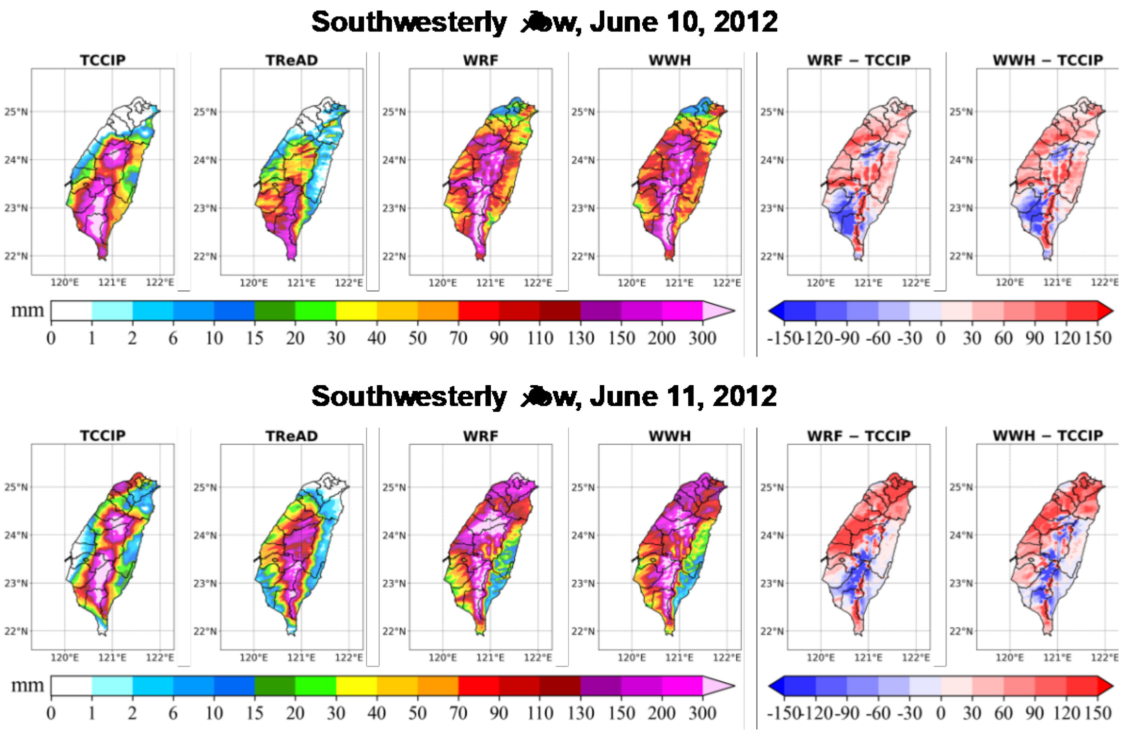

Fig. 6. As in Fig. 4, but for the southwesterly flow event (Case 3).

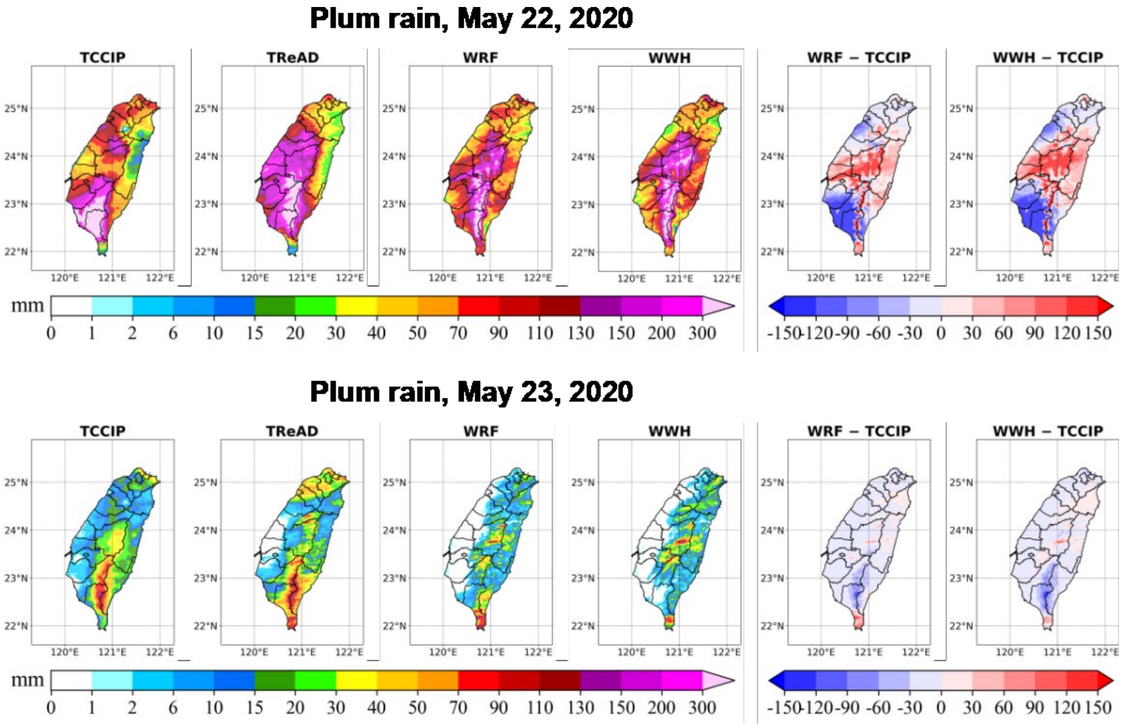

Fig. 7. As in Fig. 4, but for the plum rain event (Case 4).

Case ID & Event Date	TCCIP	WRF	WWH	TReAD
1: 2009/08/07	886.4	1770.3	1752.0	1693.5
1: 2009/08/08	1542.6	1150.6	1234.5	1949.4
2: 2010/09/19	1105.3	1748.7	1629.4	1345.1
2: 2010/09/20	288.2	435.9	497.5	591.0
3: 2012/06/10	607.7	959.7	1104.2	329.3
3: 2012/06/11	614.9	773.4	791.9	436.0
4: 2020/05/22	584.0	924.7	934.2	653.0
4: 2020/05/23	260.4	157.0	187.7	403.4

Table 3. Maximum cumulative rainfall (mm) per day for each event.

To further analyze the difference between the uncoupled and coupled simulations, the precipitation of the WWH simulation is subtracted from that of the WRF-only simulation, as shown in Fig. 8. In Cases 1 and 2 (Typhoons Morakot and Fanapi), the WRF-only simulation generally produces higher precipitation in the western-to-southwestern Taiwan and lower precipitation in the eastern Taiwan. In Case 3, higher precipitation is found in the northern and central regions in the WRF-only simulation, whereas Case 4 shows the nearly opposite pattern. While both Cases 3 and 4 occurred during the plum rain (mei-yu) season when a quasi-stationary front (mei-yu front) associated with strong southwesterly winds is commonly found, the two cases were characterized by distinctive large-scale meteorological patterns and event progressions. On the first day of Case 3 (June 10, 2012), high southwesterly moisture fluxes transported from the Indian Ocean and the Bay of Bengal and lifted by Taiwan's terrain (orographic effects) induced heavy rainfall in the windward side of central and southern Taiwan. On Day 2 (June 11, 2012), apart from the orographic effects, the northwestern coast of Taiwan started receiving heavy rainfall due to the enhanced convective activities by the localized convergence between the southwesterly "barrier jet (Chen and Li, 1995; Li and Chen 1998; Yeh and Chen, 2003)" and environmental airflow (Chen et al., 2018; Ke et al., 2019). In contrast, on the first day of Case 4 (May 22, 2020), heavy rainfall in southern Taiwan was mainly induced by the mesoscale convective systems, which were triggered over the upstream ocean (southwest to Taiwan) where the southwesterly flow was lifted by the mei-yu front. Further, Chien and Chiu (2023) indicated that there was a "southwest vortex" determining the direction of upstream flow in favor of generating the heavy rainfall area. The rainband then quickly moved southward to the Bashi Channel on Day 2 (May 23, 2020), largely reducing the amount of rainfall in southern Taiwan.

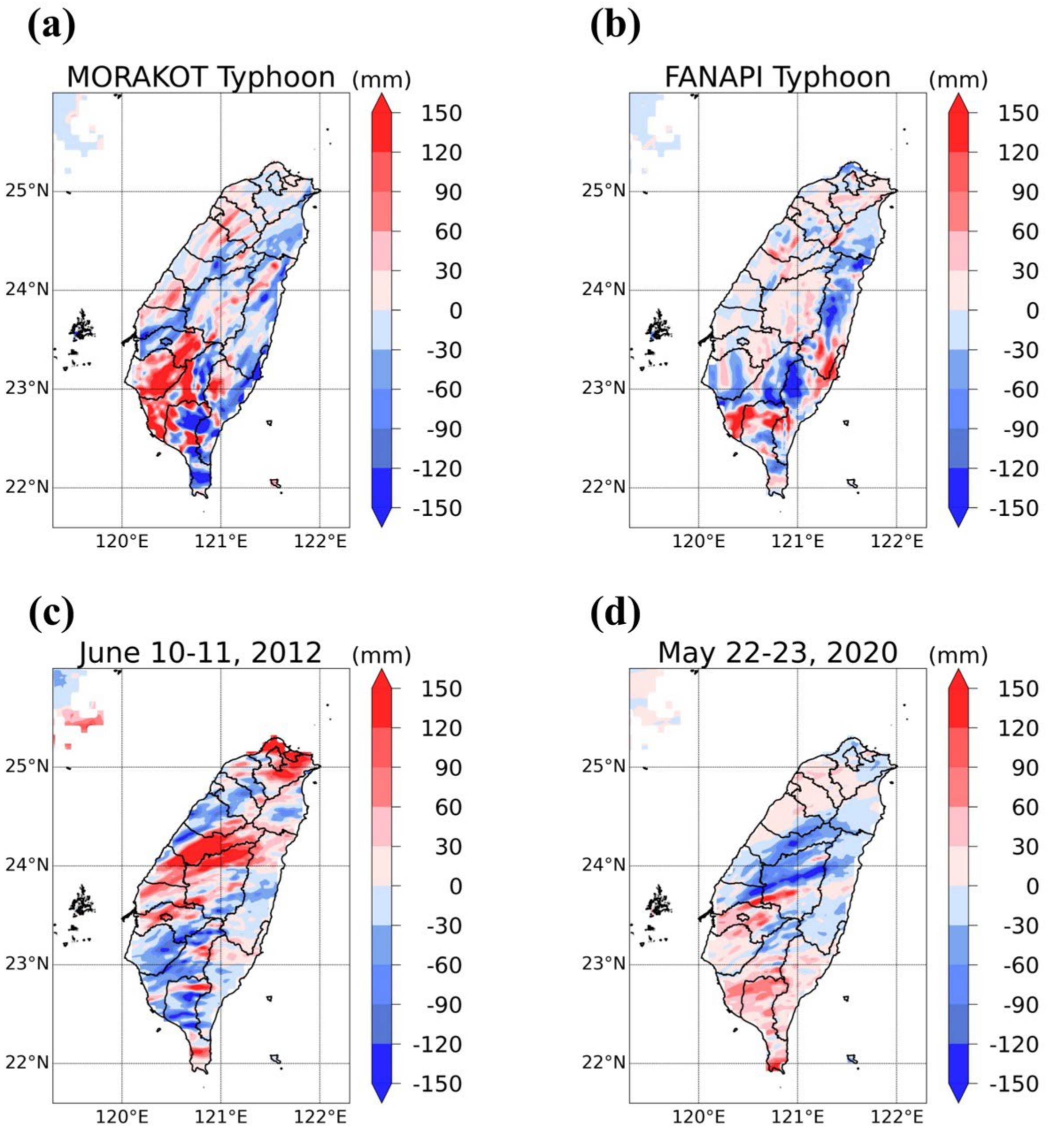

Fig. 8. Difference between the WRF-only and WWH simulated precipitation (former minus later) for the four selected cases.

Given the distinctive large-scale background, the somewhat opposite pattern between Figs. 8c (Case 3) and 8d (Case 4) can be attributed to the different model responses to land surface conditions. The enhanced flow routing scheme in the WWH configuration can alter the land surface conditions (e.g., soil moisture) during the simulations, thereby affecting land-atmosphere interactions and precipitation (Chen et al., 2023). It is generally acknowledged that anomalous high soil moisture can induce stronger local convection (Pal and Eltahir, 2001; Taylor et al., 2011; Zhao et al., 2022). Therefore, Zone A1 in Fig. 9a shows a higher soil moisture zone in the WRF-only simulation that should partially account for the higher precipitation over the same area in Fig. 8c. Zones A2 and B in Fig. 9 suggest the opposite, where the prominently lower soil moisture zones in the WRF-only simulation are found and related to the milder local convection compared to the WWH simulation. While straightforward, the effect of soil moisture on precipitation is often countervailed or superseded by larger-scale systems; this is why we observed no significant differences in precipitation on Day 1 of Cases 3 and 4 when the major source of moisture is carried over from the upstream ocean. In sum, these results indicate that the precipitation differences between the uncoupled and coupled simulations can be significant (up to ~150 mm), highlighting the importance of detailed hydro-meteorological processes and related parameterization schemes. Further investigations are required to understand the varied patterns of these differences in simulated precipitation and their intricate relationship with coupled model physics.

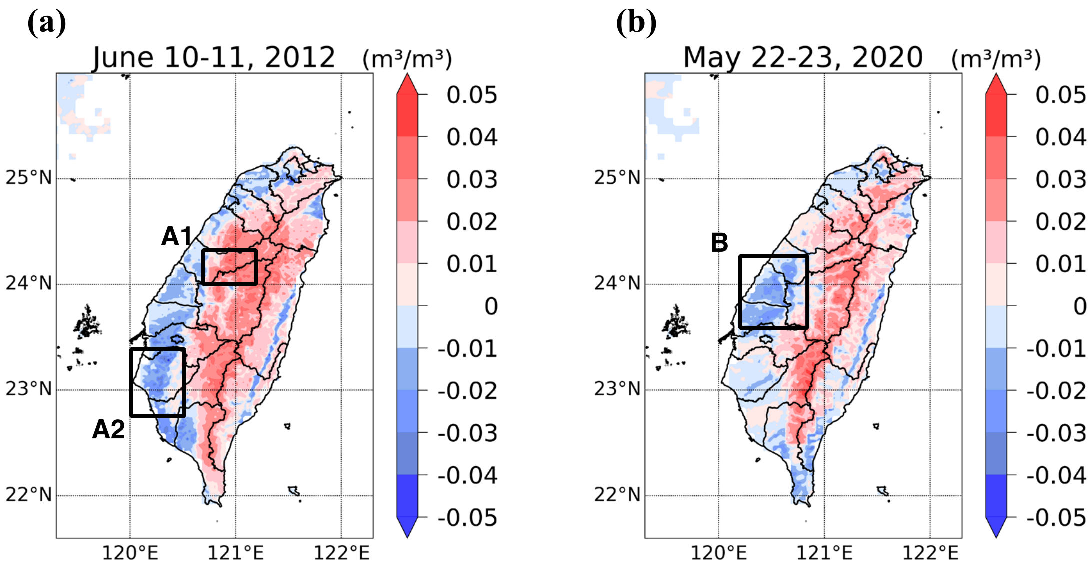

Fig. 9. Difference between the WRF-only and WWH simulated soil moisture (former minus later) for (a) Case 3 and (b) Case 4.

The results of the streamflow simulations are examined, as the performance is crucial for the subsequent TRITON inundation modeling. The hydrographs simulated by WWH are compared with observed data, as shown in Fig. 10. It can be seen that the simulated streamflow is overestimated in most cases, likely due to the previously discussed overestimation of rainfall predicted by WWH. Although the overestimated rainfall directly impacts streamflow predictions, a few stations still demonstrate reasonable performance. For instance, the correlation coefficient between the observed and simulated hydrographs at the

Nanxiong Bridge station for Case 1 is 0.76 (Fig. 10b), and at the Shanlin Bridge station for Case 4 is 0.74 (Fig. 10h). In addition to the uncertainty of rainfall prediction, the coarse resolution of the DEM (HydroSHED) may also cause inaccurate streamflow simulations (Kim et al., 2021). While HydroSHED offers stable and efficient simulation in WRF-Hydro, it may be worthwhile to explore using a higher-resolution, hydrologically conditioned DEM in the future.

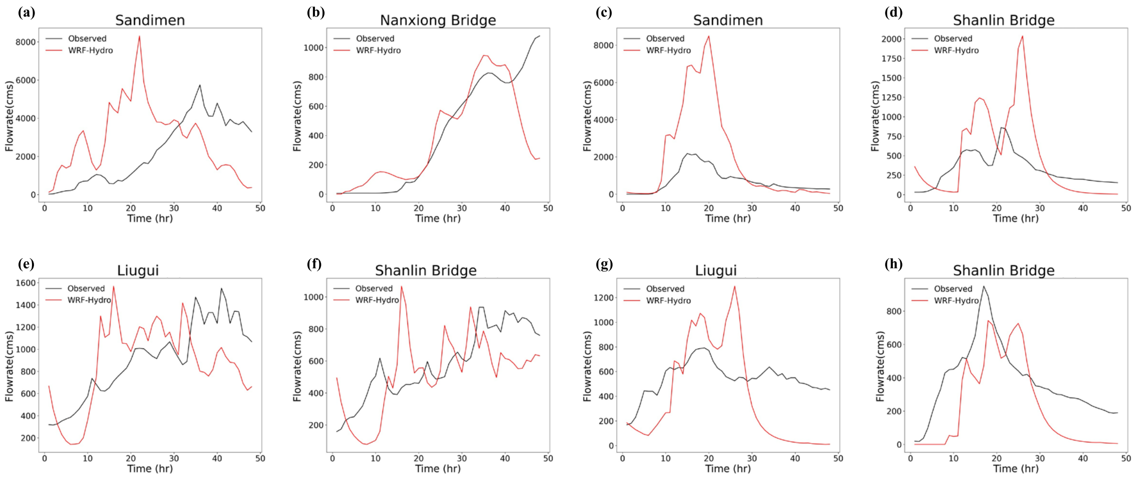

Fig. 10. Observed vs. simulated streamflow hydrographs using WWH for the four selected cases: (a) and (b) Typhoon Morakot, (c) and (d) Typhoon Fanapi, (e) and (f) southwesterly flow, and (g) and (h) plum rain.

b. Inundation simulation

1) Coupled WWH and TRITON simulation

Before conducting the one-way coupling of WWH with TRITON, we first perform the verification of TRITON. Although it would be better to compare TRITON-simulated surface water levels with observations, there is no continuous record of observed water levels for historical flood events in Taiwan. To verify the performance of TRITON in the absence of observed water levels, we thus opt for a flood map comparison between the TRITON-based and official products, assuming the official flood map represents the most accurate flood pattern subject to the design storm. The official flood map of Kaohsiung City, a special municipality in the Gaoping region, was developed by Taiwan's WRA using the SOBEK model with a 24-hr, 650-mm design storm, which accounted for specific flood control facilities (e.g., drainage ways and levees) and sewage systems. In our verification of TRITON, we adopt an effective rainfall approach that simply reduces the input rainfall to

TRITON by a constant percentage (similar to the Φ-index method; Mays, 2019) to mimic the attenuation effect of flood control facilities. We also exclude water bodies (e.g., reservoirs, channels, and rivers) from the flood extent based on the NLSC land use data. Despite the differences between SOBEK and TRITON, the flood map generated by TRITON bears a notable resemblance to that by SOBEK in terms of spatial patterns and magnitude (Fig. S1 in the supplemental material). The high resemblance thus ensures the capability and reliability of TRITON, which has thus far been configured. It is important to note that our verification is intended to evaluate TRITON's overall performance. A more quantitative comparison between the SOBEK and TRITON simulations could be made once detailed flood control facilities are modeled and included in TRITON in future developments.

After verifying TRITON, we can use the simulated streamflow hydrograph from each case in WWH to drive TRITON for inundation simulation. The maximum flood depth of each grid in the domain can be obtained from the simulation, as shown in Fig. 11, where the survey data compiled by Taiwan's WRA are also overlaid. It should be noted that the survey data only present coarse-scale flood extent (without flood depth information), and fine-scale, localized flooding, as well as low-lying farms and fish farms, are not included in the survey data. As shown in the figure, the simulated inundation areas for Typhoons Morakot and Fanapi are similar to the survey data to a certain extent, especially in metropolitan areas such as Luzhu, Gangshan, Nanzi, Zuoying, Dashe, Renwu, Qishan, and Meinong Districts. However, notable fluvial flooding in certain areas, such as Daliao and Linyuan District, differs from the survey data, likely due to the absence of a levee (flood defense) module in the current version of TRITON. Such an issue could be addressed by raising/modifying local DEM, which is currently under inspection. Cases 3 and 4 only show sporadic and localized areas affected by flooding, and the coupled simulation results of WWH and TRITON also indicate very slight flooding (Fig. S2 in the supplemental material). Additionally, according to NCDR's disaster records and reports, there were actual flooding impacts in Nanzi, Gushan, and Yancheng Districts, where TRITON has successfully simulated flooding in Case 3.

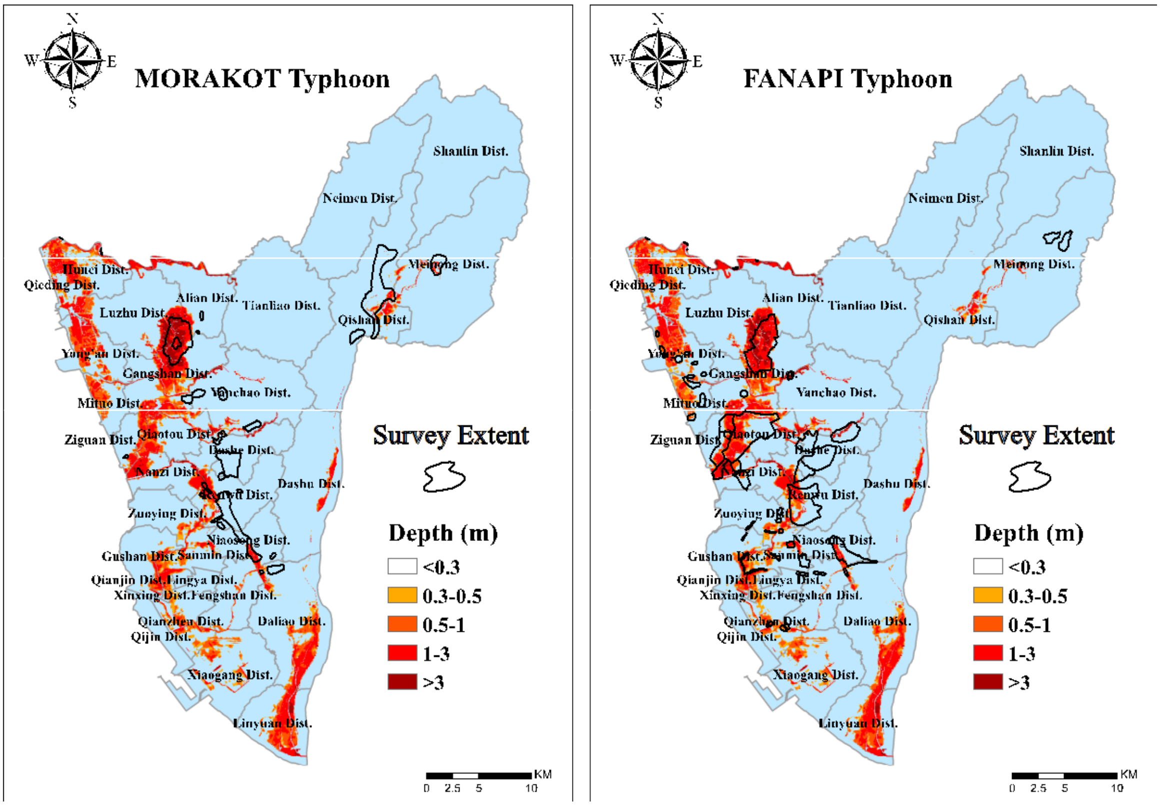

Fig. 11. Maximum flood depth derived from TRITON simulations, overlaid with the survey extent for Typhoons Morakot and Fanapi (Cases 1 and 2).

Despite the uncertainty of rainfall and streamflow prediction in each case, the inundation simulation successfully identified flooding hotspots with a high degree of similarity to the survey data. These flooding hotspots represent flood-prone areas; in other words, as long as the simulated rainfall and streamflow remain within a valid range, flooding in these areas can be triggered. Our proposed modeling framework that successfully identifies flooding hotspots manifests how simulation biases propagate along the three levels of model cascades (i.e., WRF, WRF-Hydro, and TRITON). We find the amplified biases from the WRF-based QPFs to the WRF-Hydro-based streamflow predictions, but the propagated biases could be reverted in the TRITON-based flood predictions run with a finer resolution DEM. Our finding in Taiwan is also corroborated by Rodríguez-Rincón et al. (2015) and Gangrade et al. (2023), who conducted flood simulations in the southeast of Mexico and Central Tennessee, respectively. Therefore, even though there are uncertainties in some forecasting aspects (e.g., flood depth and the exact timing of peak flooding), the coupled modeling framework proposed in this study appears to be sensitive enough to forecast large flooding events on a coarse scale and to reflect minor flooding events of lower rainfall-streamflow intensity. This capability should be beneficial for operational forecasting.

2) Efficiency and sensitivity of TRITON

To further demonstrate the applicability of the proposed modeling framework for real-time operational forecasting, we evaluate the efficiency of TRITON simulation by exploring the effect of different grid resolutions and hardware configurations on flood simulations. Using Typhoon Fanapi as the test case, we simulate with six grid resolutions (i.e., 15, 20, 30, 50, 70, and 90 m) on a Linux server equipped with an NVIDIA TITAN RTX GPU, an Intel(R) Xeon(R) Gold 6230R CPU @ 2.10GHz, and 128GB memory. The number of simulation grids and elapsed real time are summarized in Table 4, with the speed-up factor defined as the CPU simulation time divided by the GPU simulation time. In our experiment, the speed-up factor increases significantly with the number of simulation grids and can reach as high as ~13.

Grid Resolution	Num. Grids (million)	Elapsed Real Time using GPU (hr)	Elapsed Real Time using CPU (hr)	Speed-up Factor
15 m	46.7	8.2	107.5	13.1
20 m	26.3	3.5	42.3	12.1
30 m	11.6	1.1	11.5	10.4
50 m	4.2	0.3	2.2	7.3
70 m	2.1	0.1	0.6	6.0
90 m	1.2	0.06	0.17	2.8

Table 4. Relationship between the grid resolution (number of grids) and elapsed real time under different hardware implementations (i.e., GPU vs. CPU).

Different grid sizes also have a direct impact on the accuracy of flood simulations. Table 5 shows that larger grid sizes (coarser resolutions) tend to create a larger inundation area of a high flood depth (> 3 m). Additionally, larger grid sizes are more likely to cause excessive averaging of elevation, leading to unrealistic terrain changes and unstable simulation results. For example, by zooming in on the simulation results at different resolutions in Luzhu, Alian, and Gangshan Districts (Fig. 12), it becomes clear that smaller grid sizes (finer resolutions) better depict the actual flooding situation. Therefore, due to the significant increase in simulation efficiency, using GPU-accelerated TRITON is one of the most promising approaches to provide timely flood forecasting at sufficient resolution in response to more extreme weather conditions.

Grid Resolution	A ($h < 0.3$)	A ($0.3 \leq h < 0.5$)	A ($0.5 \leq h < 1.0$)	A ($1.0 \leq h < 3.0$)	A ($h > 3.0$)
15 m	501.2	21.4	44.3	60.7	9.7
20 m	487.3	22.1	46.7	71.6	10.1
30 m	484.9	21.3	52.2	68.8	10.6
50 m	481.5	23.3	51.7	71.5	10.1
70 m	481.8	21.7	55.2	68.0	11.4
90 m	490.0	25.0	48.1	63.3	12.0

Table 5. Relationship between the grid resolution and inundation area (A, in square kilometers) under different flood depth intervals (h, in meters).

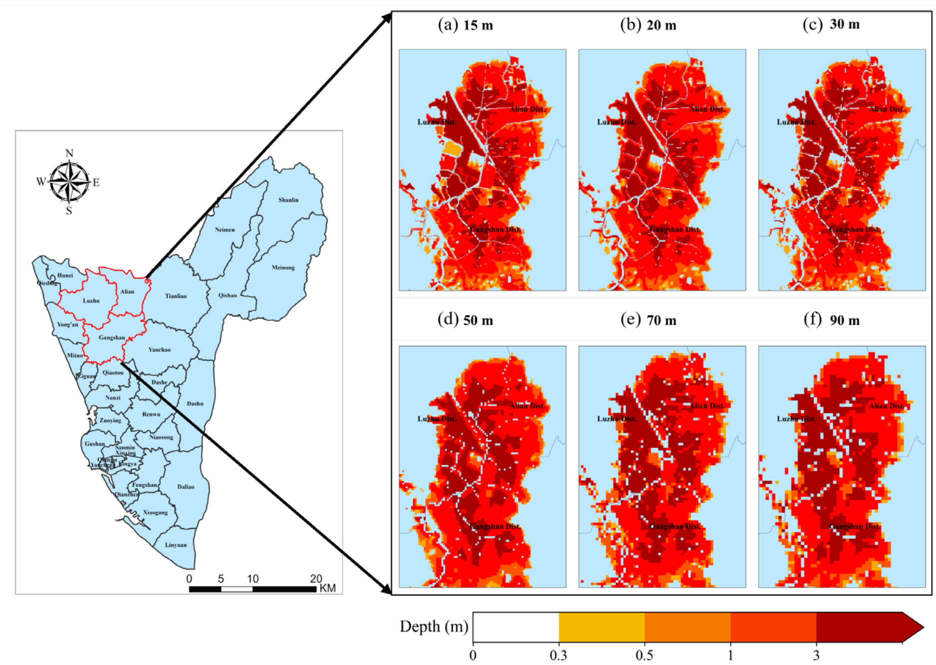

Fig. 12. Simulation results of maximum flood depth at different grid resolutions in Luzhu, Alian, and Gangshan Districts. (a) to (f) represent grid resolutions from 15 to 90 m, corresponding to Table 5.

5. Concluding remarks

The increased frequency of extreme rainfall due to climate change has underscored the need for more effective flood modeling capabilities. In this study, we evaluated the performance of atmospheric-hydrological forcings (i.e., rainfall and streamflow) simulated by the WWH model, and then used these forcings to drive the TRITON model to assess the regional inundation in the Gaoping region over southwestern Taiwan. Our numerical experiment included four heavy-to-torrential rainfall cases representing the major rainfall types in Taiwan. The efficiency and sensitivity of TRITON were also examined. After conducting these multi-faceted and coupled-modeling evaluations, we summarize our major findings as follows:

1. The rainfall simulation results indicated that the spatial pattern of rainfall across the entire island of Taiwan is generally reasonable when compared to observed rainfall. However, the pattern and amount of rainfall in the Gaoping region still require improvement. The WWH simulations overestimated rainfall in certain areas compared to the TReAD results.
2. The discrepancies in simulated rainfall and the resolution of the DEM contributed to the expected differences between the simulated and observed streamflow. Despite uncertainties in the simulated rainfall and streamflow, coupling WWH with TRITON to simulate the selected flood events can effectively identify the main inundation hotspots in the study area.
3. Testing different grid resolutions and hardware configurations for TRITON simulations revealed that GPU-based simulations were significantly more efficient than CPU-based ones, achieving a speed-up factor as high as ~13. This improved efficiency highlights the need for an HPC modeling framework like the one proposed in this study, particularly because the accuracy of flood simulations depends on using a finer resolution DEM.

According to our case study, the coupled atmospheric-hydrological and high-performance hydrodynamic modeling framework has demonstrated rapid and feasible flood prediction despite several identified uncertainties. For hydrologic forcings, other atmospheric data sources besides FNL (e.g., ERA5 and GFS) could be used as different initial and boundary conditions to explore the uncertainty of rainfall simulation and to consider other possible inundation scenarios. Additionally, this modeling framework could be integrated with emerging monitoring techniques (e.g., IoT, UAV devices) to enhance further the effectiveness of early warning systems, such as by implementing real-time corrections to flood forecasts.

Acknowledgments.

We are grateful to the NLSC for providing the land use data, the Central Weather Agency and TCCIP for providing the rainfall data, and the WRA for providing the streamflow data. SCK is employed by UT-Battelle, LLC, under contract DE-AC05-00OR22725 with the US Department of Energy (DOE). Correspondingly, the US government retains and the publisher, by accepting the article for publication, acknowledges that the US government retains a nonexclusive, paid-up, irrevocable, worldwide license to publish or reproduce the published form of this manuscript, or allow others to do so, for US government purposes. DOE will provide public access to these results of federally sponsored research in accordance with the DOE Public Access Plan (https://www.energy.gov/doe-public-access-plan).

Data Availability Statement.

The numerical model simulations upon which this study is based are too large to archive or to transfer. Instead, we provide all the information needed to replicate the simulations; we used WRF version 4.2.1, WRF-Hydro version 5.1.1, and TRITON version 1.0. The model codes of WRF, WRF-Hydro, and TRITON are available at https://github.com/wrf-model/WRF, https://github.com/NCAR/wrf_hydro_nwm_public, and https://code.ornl.gov/hydro/triton, respectively. Other data used and analyzed in this study (e.g., data preprocessing codes, postprocessing codes, and the namelist settings) are available from the corresponding author (cjchen@nchu.edu.tw) upon reasonable request.

SUPPLEMENTAL MATERIAL

The following supporting information is stored in a separate file: Table S1 and Figures S1 and S2.

REFERENCES

Asghar, M. R., T. Ushiyama, M. Riaz, and M. Miyamoto, 2019: Flood and inundation forecasting in the sparsely gauged transboundary Chenab River basin using satellite rain and coupling meteorological and hydrological models. *J. Hydrometeor.*, **20**(12), 2315–2330.

Brunner, G. W., 2016: *HEC-RAS river analysis system: hydraulic reference manual, version 5.0.*, US Army Corps of Engineers–Hydrologic Engineering Center, 547 pp.

Chen, C. J., C. C. Chen, M. H. Lo, J. Y. Juang, and C. M. Chang, 2020: Central Taiwan's hydroclimate in response to land use/cover change. *Environ. Res. Lett.*, **15**(3), 034015.

Chen, C. J., M. H. Chi, and J. R. Ye, 2023: Assessing hydroclimate response to land use/cover change using coupled atmospheric-hydrological models. *Geosci. Lett.*, **10**(1), 54.

Chen, Y. L., and J. Li, 1995: Large-scale conditions favorable for the development of heavy rainfall during TAMEX IOP 3. *Mon. Weather Rev.*, **123**(10), 2978–3002.

Chen, Y. L., Y. J. Chu, C. S. Chen, C. C. Tu, J. H. Teng, and P. L. Lin, 2018: Analysis and simulations of a heavy rainfall event over northern Taiwan during 11–12 June 2012. *Mon. Weather Rev.*, **146**(9), 2697–2715.

Chen, Y. Y., W. Huang, W. H. Wang, J. Y. Juang, J. S. Hong, T. Kato, and S. Luyssaert, 2019: Reconstructing Taiwan's land cover changes between 1904 and 2015 from historical maps and satellite images. *Sci. Rep.*, **9**(1), 3643.

Chien, F. C., Y. H. Kuo, and M. J. Yang, 2002: Precipitation forecast of MM5 in the Taiwan area during the 1998 Mei-yu season. *Weather Forecast.*, **17**(4), 739–754.

Chien, F. C., and Y. C. Chiu, 2023: Factors leading to heavy rainfall in Southern Taiwan in the early mei-yu season of 2020. *Mon. Weather Rev.*, **151**(7), 1885–1908.

Cvetkovic, V. M., and J. Martinović, 2020: Innovative solutions for flood risk management. *Int. J. Disaster Risk Manag.*, **2**(2), 71–100.

Dottori, F., W. Szewczyk, J.C. Ciscar, F. Zhao, L. Alfieri, Y. Hirabayashi, A. Bianchi, I. Mongelli, K. Frieler, R.A. Betts, and L. Feyen, 2018: Increased human and economic losses from river flooding with anthropogenic warming. *Nat. Clim. Change*, **8**(9), 781–786.

Dowell, D. C., C. R. Alexander, E. P. James, S. S. Weygandt, S. G. Benjamin, G. S. Manikin, B. T. Blake, J. M. Brown, J. B. Olson, M. Hu, and T. G. Smirnova, 2022: The High-Resolution Rapid Refresh (HRRR): An hourly updating convection-allowing forecast model. Part I: Motivation and system description. *Weather Forecast.*, **37**(8), 1371–1395.

Dullo, T. T., G, K. Darkwah, S. Gangrade, M. Morales-Hernández, M. B. Sharif, A. J. Kalyanapu, S. C. Kao, S. Ghafoor, and M. Ashfaq, 2021: Assessing climate-change-induced flood risk in the Conasauga River watershed: an application of ensemble hydrodynamic inundation modeling. *Nat. Hazards Earth Syst. Sci.*, **21**(6), 1739–1757.

Eltahir, E. A., and R. L. Bras., 1996: Precipitation recycling. *Rev. Geophys.*, **34**(3), 367–378.

European Centre for Medium-Range Weather Forecasts (ECMWF). 2017: updated monthly. ERA5 Reanalysis. Research Data Archive at the National Center for Atmospheric Research, Computational and Information Systems Laboratory. https://doi.org/10.5065/D6X34W69.

Galanaki, E., K. Lagouvardos, V. Kotroni, T. Giannaros, and C. Giannaros, 2021: Implementation of WRF-Hydro at two drainage basins in the region of Attica, Greece, for operational flood forecasting. *Nat. Hazards Earth Syst. Sci.*, **21**(7), 1983–2000.

Gangrade, S., G. R. Ghimire, S. C. Kao, M. Morales-Hernández, A. A. Tavakoly, J. L. Gutenson, K. H. Sparrow, G. K. Darkwah, A. J. Kalyanapu, and M. L. Follum, 2023: Unraveling the 2021 Central Tennessee flood event using a hierarchical multi-model inundation modeling framework. *J. Hydrol.*, **625**, p.130157.

Gochis, D. J., M. Barlage, R. Cabell, M. Casali, A. Dugger, K. FitzGerald, M. McAllister, J. McCreight, A. RafieeiNasab, L. Read, K. Sampson, D. Yates, and Y. Zhang, 2020: *The WRF-Hydro® modeling system technical description (Version 5.1.1)*. NCAR Technical Note. 108 pages. Available online at: https://ral.ucar.edu/sites/default/files/public/WRFHydroV511TechnicalDescription.pdf.

Hong, J. S., 2003: Evaluation of the high-resolution model forecasts over the Taiwan area during GIMEX. *Weather Forecast.*, **18**(5), 836–846.

Hsiao, L. F., M. J. Yang, C. S. Lee, H. C. Kuo, D. S. Shih, C. C. Tsai, C. J. Wang, L. Y. Chang, D. Y. C. Chen, L. Feng, and J. S. Hong, 2013: Ensemble forecasting of typhoon rainfall and floods over a mountainous watershed in Taiwan. *J. Hydrol.*, **506**, 55–68.

Huang, H., H. Cui, and Q. Ge, 2021: Assessment of potential risks induced by increasing extreme precipitation under climate change. *Nat. Hazards*, **108**(2), 2059–2079.

Huang, S. H., K. Mahmud, and C. J. Chen, 2022: Meaningful trend in climate time series: A discussion based on linear and smoothing techniques for drought analysis in Taiwan. *Atmos.*, **13**(3), 444.

James, E. P., C. R. Alexander, D. C. Dowell, S. S. Weygandt, S. G. Benjamin, G. S. Manikin, J. M. Brown, J. B. Olson, M. Hu, T. G. Smirnova, and T. Ladwig, 2022: The High-Resolution Rapid Refresh (HRRR): an hourly updating convection-allowing forecast model. Part II: Forecast performance. *Weather Forecast.*, **37**(8), 1397–1417.

Janizadeh, S., S. C. Pal, A. Saha, I. Chowdhuri, K. Ahmadi, S. Mirzaei, A. H. Mosavi, and J. P. Tiefenbacher, 2021: Mapping the spatial and temporal variability of flood hazard affected by climate and land-use changes in the future. *J. Environ. Manag.*, **298**, 113551.

Kim, S., H. Shen, S. Noh, D. J. Seo, E. Welles, E. Pelgrim, A. Weerts, E. Lyons, and B. Philips, 2021: High-resolution modeling and prediction of urban floods using WRF-Hydro and data assimilation. *J. Hydrol.*, **598**, 126236.

Kundzewicz, Z. W., S. Kanae, S. I. Seneviratne, J. Handmer, N. Nicholls, P. Peduzzi, R. Mechler, L. M. Bouwer, N. Arnell, K. Mach, and R. Muir-Wood, 2014: Flood risk and climate change: global and regional perspectives. *Hydrol. Sci. J.*, **59**(1), 1–28.

Lee, T. Y., C. C. Chiu, C. J. Chen, C. Y. Lin, and F. K. Shiah, 2023: Assessing future availability of water resources in Taiwan based on the Budyko framework. *Ecol. Indic.*, **146**, 109808.

Lehner, B., K. Verdin, and A. Jarvis, 2008: New global hydrography derived from spaceborne elevation data. *Eos, Trans. Am. Geophys. Union*, **89**(10), 93–94.

Li, J., and Y. L. Chen, 1998: Barrier jets during TAMEX. *Mon. Weather Rev.*, **126**(4), 959–971.

Li, P. L., L. F. Lin, and C. J. Chen, 2021a: Hydrometeorological assessment of satellite and model precipitation products over Taiwan. *J. Hydrometeor.*, **22**(11), 2897–2915.

Li, X., C. Rankin, S. Gangrade, G. Zhao, K. Lander, N. Voisin, M. Shao, M. Morales-Hernández, S. C. Kao, and H. Gao, 2021b: Evaluating precipitation, streamflow, and inundation forecasting skills during extreme weather events: A case study for an urban watershed. *J. Hydrol.*, **603**, 127126.

Lin, P., M. A. Rajib, Z. L. Yang, M. Somos-Valenzuela, V. Merwade, D. R. Maidment, Y. Wang, and L. Chen, 2018: Spatiotemporal evaluation of simulated evapotranspiration and streamflow over Texas using the WRF-Hydro-RAPID modeling framework. *J. Am. Water Resour. Assoc.*, **54**(1), 40–54.

Livneh, B., P. J. Restrepo, and D. P. Lettenmaier, 2011: Development of a unified land model for prediction of surface hydrology and land-atmosphere interactions. *J. Hydrometeor.*, **12**(6), 1299–1320.

Ke, C. Y., K. S. Chung, T. C. Chen Wang, and Y. C. Liou, 2019: Analysis of heavy rainfall and barrier-jet evolution during Mei-Yu season using multiple Doppler radar retrievals: A case study on 11 June 2012. *Tellus A: Dyn. Meteorol. Oceanogr.*, **71**(1), p.1571369.

Mays, L. W., 2019: *Water Resources Engineering*, 3rd Ed., John Wiley & Sons, 752 pp.

Morales-Hernández, M., K. J. Evans, S. Gangrade, S. C. Kao, M. B. Sharif, S. K. Ghafoor, A. J. Kalyanapu, and T. T. Dullo, 2020: TRITON, Computer Software, Oak Ridge National Laboratory, TN, https://doi.org/10.11578/dc.20201001.85.

Morales-Hernández, M., M. B. Sharif, A. Kalyanapu, S. K. Ghafoor, T. T. Dullo, S. Gangrade, S. C. Kao, M. R. Norman, and K. J. Evans, 2021: TRITON: A Multi-GPU open source 2D hydrodynamic flood model. *Environ. Model. Softw.*, **141**, 105034.

Moriasi, D. N., M. W. Gitau, N. Pai, and P. Daggupati, 2015: Hydrologic and water quality models: Performance measures and evaluation criteria. *Trans. ASABE*, **58**(6), 1763–1785.

Pal, J. S., and E. A. Eltahir, 2001: Pathways relating soil moisture conditions to future summer rainfall within a model of the land-atmosphere system. *J. Climate*, **14**(6), 1227–1242.

Pal, S. C., I. Chowdhuri, B. Das, R. Chakrabortty, P. Roy, A. Saha, and M. Shit, 2022: Threats of climate change and land use patterns enhance the susceptibility of future floods in India. *J. Environ. Manag.*, **305**, 114317.

Papaioannou, G., G. Varlas, G. Terti, A. Papadopoulos, A. Loukas, Y. Panagopoulos, and E. Dimitriou, 2019: Flood inundation mapping at Ungauged basins using coupled

Hydrometeorological–hydraulic Modelling: The catastrophic case of the 2006 flash flood in Volos City, Greece. *Water*, **11**(11), 2328.

Rodríguez-Rincón, J. P., A. Pedrozo-Acuña, and J. A. Breña-Naranjo, 2015: Propagation of hydro-meteorological uncertainty in a model cascade framework to inundation prediction. *Hydrol. Earth Syst. Sci.*, **19**(7), 2981–2998.

Shih, D. S., C. H. Chen, and G. T. Yeh, 2014: Improving our understanding of flood forecasting using earlier hydro-meteorological intelligence. *J. Hydrol.*, **512**, 470–481.

Silver, M., A. Karnieli, H. Ginat, E. Meiri, and E. Fredj, 2017: An innovative method for determining hydrological calibration parameters for the WRF-Hydro model in arid regions. *Environ. Model. Softw.*, **91**, 47–69.

Skamarock, W. C., J. B. Klemp, J. Dudhia, D. O. Gill, D. M. Barker, M. G. Duda, X. Y. Huang, W. Wang, and J. G. Powers, 2008: A description of the advanced research WRF version 3. *NCAR technical note*, 475(125), 10-5065.

Tabari, H., 2020: Climate change impact on flood and extreme precipitation increases with water availability. *Sci. Rep.*, **10**(1), 13768.

Taylor, C. M., A. Gounou, F. Guichard, P. P. Harris, R. J. Ellis, F. Couvreux, and M. De Kauwe, 2011: Frequency of Sahelian storm initiation enhanced over mesoscale soil-moisture patterns. *Nature Geosci.*, **4**(7), 430–433.

Teng, J., A. J. Jakeman, J. Vaze, B. F. Croke, D. Dutta, and S. J. E. M. Kim, 2017: Flood inundation modelling: A review of methods, recent advances and uncertainty analysis. *Environ. Model. Softw.*, **90**, 201–216.

Varlas, G., A. Papadopoulos, G. Papaioannou, and E. Dimitriou, 2021: Evaluating the forecast skill of a hydrometeorological modelling system in Greece. *Atmos.*, **12**(7), 902.

Wang, C. C., F. C. Chien, S. Paul, D. I. Lee, and P. Y. Chuang, 2017: An evaluation of WRF rainfall forecasts in Taiwan during three mei-yu seasons from 2008 to 2010. *Weather Forecast.*, **32**(4), 1329–1351.

Wang, W., J. Liu, C. Li, Y. Liu, F. Yu, and E. Yu, 2020: An evaluation study of the fully coupled WRF/WRF-hydro modeling system for simulation of storm events with different rainfall evenness in space and time. *Water*, **12**(4), 1209.

Wasko, C., R. Nathan, L. Stein, and D. O'Shea, 2021: Evidence of shorter more extreme rainfalls and increased flood variability under climate change. *J. Hydrol.*, **603**, 126994.

Wehbe, Y., M. Temimi, M. Weston, N. Chaouch, O. Branch, T. Schwitalla, V. Wulfmeyer, X. Zhan, J. Liu, and A. Al Mandous, 2019: Analysis of an extreme weather event in a hyper-arid region using WRF-Hydro coupling, station, and satellite data. *Nat. Hazards Earth Syst. Sci.*, **19**(6), 1129–1149.

Xia, X., Q. Liang, and X. Ming, 2019: A full-scale fluvial flood modelling framework based on a high-performance integrated hydrodynamic modelling system (HiPIMS). *Adv. Water Resour.*, **132**, 103392.

Yang, S. Y., C. H. Chang, C. T. Hsu, and S. J. Wu, 2022: Variation of uncertainty of drainage density in flood hazard mapping assessment with coupled 1D–2D hydrodynamics model. *Nat. Hazards*, **111**(3), 2297–2315.

Yang, T. H., S. C. Yang, J. Y. Ho, G. F. Lin, G. D. Hwang, and C. S. Lee, 2015: Flash flood warnings using the ensemble precipitation forecasting technique: A case study on forecasting floods in Taiwan caused by typhoons. *J. Hydrol.*, **520**, 367–378.

Yeh, H. C., and Y. L. Chen, 2003: Numerical simulations of the barrier jet over northwestern Taiwan during the mei-yu season. *Mon. Weather Rev.*, **131**(7), 1396–1407.

Yucel, I., A. Onen, K. K. Yilmaz, and D. J. Gochis, 2015: Calibration and evaluation of a flood forecasting system: Utility of numerical weather prediction model, data assimilation and satellite-based rainfall. *J. Hydrol.*, **523**, 49–66.

Zhao, C., X. Meng, Y. Li, S. Lyu, J. Guo, and H. Liu, 2022: Impact of soil moisture on afternoon convection triggering over the Tibetan Plateau based on 1-D boundary layer model. *J. Geophys. Res.: Atmos.*, **127**(2), p.e2021JD035591.